Molecular Therapy
Original Article

Transcriptional intermediary factor 1 gamma prevents lung inflammation and fibrosis via AT2 cells, fibroblasts, and macrophages

Dodam Moon,[3] Hyomin Park,[3] Tae Yoon Kim,[3] Areum Cha,[1] Youngmin Kim,[1] Jaewon Lee,[2] Joong-Yub Kim,[4] Samina Park,[5] Sung-Hye Park,[6] Jaemoon Koh,[6] Kyongman An,[10] Nam-Joon Cho,[8,9] Taehoon Kim,[7] Eun Ju Lee,[1,2,11] and Hyo-Soo Kim[1,2,3,11]

[1]Interdisciplinary Program in Stem Cell Biology, Seoul National University of Medicine, Seoul 03080, Republic of Korea; [2]Biomedical Research Institute, Seoul National University Hospital, Seoul 03080, Republic of Korea; [3]Department of Molecular Medicine and Biopharmaceutical Sciences, Graduate School of Convergence Science and Technology, Seoul National University, Seoul 03080, Republic of Korea; [4]Division of Pulmonary and Critical Care Medicine, Department of Internal Medicine, Seoul 03080, Republic of Korea; [5]Department of Thoracic and Cardiovascular Surgery, Seoul 03080, Republic of Korea; [6]Department of Pathology, Seoul National University College of Medicine, Seoul 03080, Republic of Korea; [7]Department of Research and Development, LUCA AICell, Anyang 14055, Republic of Korea; [8]School of Materials Science and Engineering, Nanyang Technological University, 50 Nanyang Avenue, Singapore 639798, Singapore; [9]Centre for Cross Economy Global, School of Biological Sciences (SBS)-01s-50, 60 Nanyang Drive, Singapore 637551, Singapore; [10]AI-Bio Convergence Research Institute, Department of Industrial AI Engineering, Graduate School of Management of Technology, Hoseo University, Asan City 31499, Republic of Korea

Transcriptional intermediary factor 1 γ (TIF1-γ) inhibits transforming growth factor β (TGF-β) signaling, the main pathway involved in fibrosis. We previously showed that TIF1-γ regulated anti-fibrotic processes in the liver. Here, we aimed to evaluate the therapeutic potential of TIF1-γ in pulmonary fibrosis (PF). TIF1-γ inhibited the TGF-β-induced epithelial-mesenchymal transition in alveolar type 2 cells and activation of fibroblasts *in vitro*. In activated macrophages, TIF1-γ reduced inflammatory cytokine secretion. In the *in vivo* PF mice model, TIF1-γ significantly reduced fibrosis and improved lung function. In *ex vivo* fibrotic precision cut lung slices from mice and patients with PF, TIF1-γ inhibited epithelial-mesenchymal transition of epithelial cells and activation of fibroblasts and reduced inflammatory cytokine secretion in macrophages. Conclusively, TIF1-γ is a promising candidate of gene therapy for PF by modulating three cell types (alveolar type 2 cells, fibroblasts, and macrophages) involved in PF pathogenesis.

INTRODUCTION

Pulmonary fibrosis (PF) is a chronic interstitial lung disease characterized by progressive inflammation and fibrosis. As the disease progresses, lung tissue thickens and stiffens, impairing pulmonary function and eventually leading to death from respiratory failure.[1]

PF is classified into five groups: idiopathic, autoimmune related, exposure related, a mixed group of rare and ultra-rare diseases, and sarcoidosis.[2] The most common type of PF is idiopathic, occurring in approximately 5.6 cases per 100,000 people annually, with a median survival time of 3–5 years post-diagnosis and a 5-year survival rate of 20%–40%.[3–5] Continuous epithelial injury triggers epithelial-mesenchymal transition (EMT), causing excessive fibroblasts and mesenchymal cell proliferation, followed by fibroblast-myofibroblast transition (FMT). This results in the secretion of extracellular matrix (ECM) into the lung interstitium, causing structural rearrangement and worsening fibrosis.[3,5]

Transforming growth factor β (TGF-β) plays a pivotal role in fibrosis progression. It induces several critical events in the lungs: promotion of EMT in alveolar type 2 (AT2) cells, stimulation of mesenchymal cell and fibroblast proliferation leading to FMT, and induction of ECM production by myofibroblasts. TGF-β is a central mediator orchestrating multiple cellular responses contributing to PF pathogenesis.[6,7]

The anti-fibrotic drugs pirfenidone and nintedanib have been shown to slow the progression of PF and improve survival by delaying the decline in forced vital capacity and lung-diffusing capacity, thereby offering a significant benefit to patients compared to those who do not receive treatment. In previous reports, however, pirfenidone and nintedanib did not halt PF progression in more than half of the patients and caused frequent adverse events.[8,9] Another study revealed that the more advanced the lung disease, the more rapidly

Received 23 February 2025; accepted 22 August 2025;
https://doi.org/10.1016/j.ymthe.2025.08.035.

[11]These authors contributed equally

Correspondence: Eun Ju Lee, Biomedical Research Institute, Seoul National University Hospital, 101 DeaHak-ro, JongRo-gu, Seoul 03080, Republic of Korea.
E-mail: leeunju@snu.ac.kr
Correspondence: Hyo-Soo Kim, Department of Internal Medicine, Seoul National University Hospital, Molecular Medicine & Biopharmaceutical Sciences, Seoul National University, 101 DeaHak-ro, JongRo-gu, Seoul 03080, Republic of Korea.
E-mail: hyosoo@snu.ac.kr

Please cite this article in press as: Moon et al., Transcriptional intermediary factor 1 gamma prevents lung inflammation and fibrosis via AT2 cells, fibroblasts, and macrophages, Molecular Therapy (2025), https://doi.org/10.1016/j.ymthe.2025.08.035

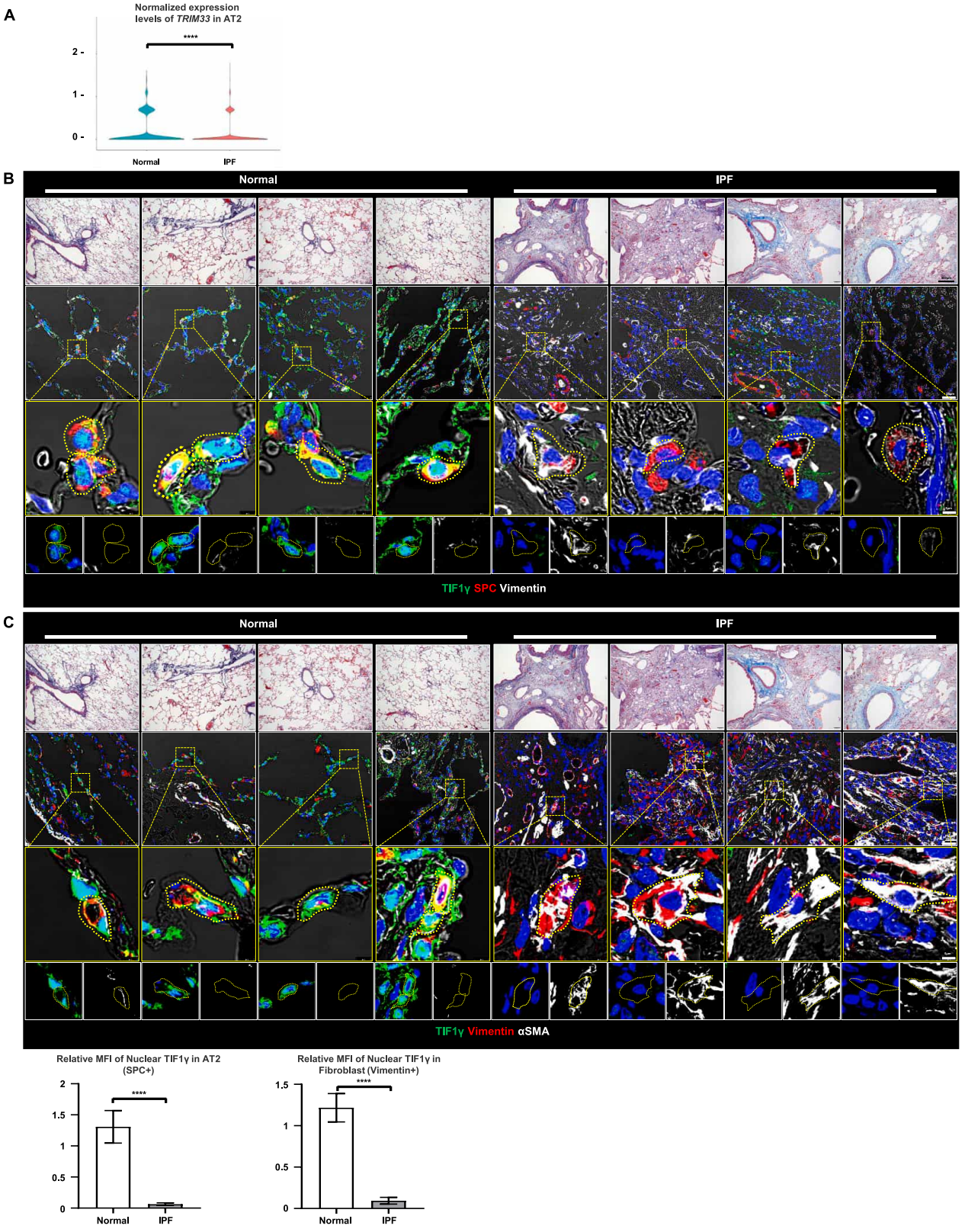

(legend on next page)

Please cite this article in press as: Moon et al., Transcriptional intermediary factor 1 gamma prevents lung inflammation and fibrosis via AT2 cells, fibroblasts, and macrophages, Molecular Therapy (2025), https://doi.org/10.1016/j.ymthe.2025.08.035

respiratory function declined.[10] Given that PF is a severe, lifelong lung disease and current anti-fibrotic drugs are only effective in half of the patients, alternative treatment approaches are required. We previously identified transcriptional intermediary factor 1 γ (TIF1-γ) as an anti-fibrotic factor inhibiting TGF-β signaling in the liver.[11] Codon optimization of TIF1-γ complementary DNA (cDNA) significantly improved protein yield, and the vector with an optimized TIF1-γ plasmid successfully demonstrated therapeutic effects against liver fibrosis.[12]

TIF1-γ functions as a transcriptional co-regulator, modulating gene expression through interactions with various proteins. Its specific role is context dependent, varying with the cellular environment and the signaling pathways involved.[13] Therefore, in this study, we aimed to prove that TIF1-γ gene therapy could be a potential treatment option for PF using pre-clinical models, including (1) TGF-β-activated AT2 cells and fibroblasts, as well as macrophages activated by lipopolysaccharide (LPS) *in vitro*, (2) a bleomycin-treated PF mouse model, and (3) precision-cut lung slices (PCLSs) from patients with PF undergoing surgery (*ex vivo* model).

RESULTS

TIF1-γ expression is reduced in AT2 cells in the lungs of patients with PF

In our previous study, hepatic stellate cells (HSCs) with stemness characteristics exhibited high levels of TIF1-γ in their quiescent state. HSCs are activated by TGF-β as fibrosis progresses, decreasing TIF1-γ expression, consequently triggering their differentiation into myofibroblasts.[11] These findings highlight the role of TIF1-γ in maintaining a quiescent state and preventing HSCs from developing into fibrogenic myofibroblasts. AT2 cells have stemness features and play crucial roles in regenerating the alveolar epithelium.[6,14] Given the functional similarities between HSCs and AT2 cells, we hypothesized that AT2 cells might also express TIF1-γ and investigated the anti-fibrosis role of TIF1-γ in AT2 cells.

Single-cell RNA sequencing (scRNA-seq) data from the Gene Expression Omnibus (GEO) database revealed a decreased *TRIM33* expression in AT2 cells of patients with PF compared to that in AT2 cells of healthy individuals (Figure 1A; Table S1). We confirmed the decreased TIF1-γ expression in AT2 cells in the lung tissues of patients with PF through immunostaining for TIF1-γ, surfactant protein C (SPC; AT2 cell marker), and vimentin (EMT marker). The reduction of TIF1-γ expression in AT2 cells was accompanied by increased vimentin expression, indicating an activated state (Figure 1B). Reduced TIF1-γ expression was also found in fibroblasts in the lungs of patients with PF, suggesting their differentiation into myofibroblasts, as shown by additional immunostaining for TIF1-γ, vimentin, and α-smooth muscle actin (αSMA, myofibroblast marker) (Figure 1C). These findings show that as PF progresses, TIF1-γ expression decreases both in AT2 cells leading to EMT and in fibroblasts leading to myofibroblasts secreting ECM. These observations in human lung tissues suggest that TIF1-γ may be an important regulator of PF.

Effect of TIF1-γ on AT2 cell and fibroblast to inhibit lung fibrosis

When TGF-β is activated, AT2 cells undergo EMT and differentiate into myofibroblasts.[15] Experiments were conducted using A549 cells, a human lung adenocarcinoma epithelial cell line widely utilized as a surrogate for AT2 cells due to their phenotypic similarity, to investigate the anti-fibrotic effect of TIF1-γ upon TGF-β stimulation.[16] The AT2 cells were transduced with lentiviruses (cytomegalovirus-red fluorescent protein [CMV-RFP], CMV-TIF1-γ-internal ribosome entry site [IRES]-tdTomato) and subsequently treated with TGF-β to activate fibrosis (Figure 2A). Quantitative polymerase chain reaction (qPCR) results showed that TGF-β-induced EMT up-regulation and *CDH1* reduction were reversed by TIF1-γ (Figure 2B). Western blotting analysis confirmed that TIF1-γ inhibited TGF-β-induced EMT at the protein level (Figure 2C). Immunofluorescence (IF) of AT2 cells overexpressing TIF1-γ revealed the sustained expression of E-cadherin and suppressed expression of N-cadherin, vimentin, and αSMA, even after TGF-β treatment (Figure 2D). The inhibitory action of TIF1-γ on TGF-β signaling in AT2 cells was supported by immunoprecipitation (IP) under TGF-β stimulation. Pull-down assays using anti-SMAD3 antibodies followed by immunoblotting detected TIF1-γ and SMAD4. The results demonstrated that TGF-β-induced interactions between SMAD3 and SMAD4 were diminished due to the interaction between SMAD3 and TIF1-γ, which aligns with the proximity ligation assay (PLA) findings (Figures 2E and S1A).

To confirm the anti-fibrotic efficacy of TIF1-γ in fibroblasts, we transduced human dermal fibroblasts (HDFs) with lentiviruses and then treated them with TGF-β. Fluorescence microscopy showed that TGF-β-treated HDFs exhibited an elongated shape demonstrating transition to myofibroblast, whereas TIF1-γ-overexpressing cells maintained a round shape (Figure 2F). Western blotting showed that the myofibroblast markers αSMA and collagen type 1α1 (Col1a1) were induced by TGF-β, which was reversed by TIF1-γ (Figure 2G). IF demonstrated that TGF-β treatment induced the expression of αSMA, Col1a1, and Ki67 (proliferative marker), as well as the elongated shape of HDF, which was reversed by

Figure 1. The expression level of transcriptional intermediary factor 1 γ is reduced in the alveolar type 2 cells of the lungs in patients with pulmonary fibrosis

(A) Single-cell RNA sequencing data shows decreased tripartite motif containing 33 (*TRIM33*) expression in alveolar type 2 (AT2) cells and fibroblast from patients with pulmonary fibrosis (PF) ($N = 12$) compared with normal individuals ($N = 10$). (B) Immunofluorescence (IF) staining for TIF1-γ, surfactant protein C (SPC), and vimentin in lung tissues from normal individuals ($N = 4$) and patients with PF ($N = 4$). SPC^+ cells indicate AT2 cells, SPC^+ $vimentin^+$ cells represent activated AT2 cells. (C) IF staining for TIF1-γ, vimentin, and α-smooth muscle actin (αSMA) in fibroblasts within the lungs of patients with PF. $Vimentin^+$ cells correspond to fibroblasts, and $vimentin^+$ $αSMA^+$ cells denote activated fibroblasts. For quantification, three (400×) images in each slide were analyzed (B′ and C′). Representative Masson's trichrome (MT) staining is shown at the top to visualize fibrotic changes in lung architecture. Data are presented as mean ± standard deviation (SD). $^*p < 0.05$; $^{**}p < 0.01$; $^{***}p < 0.001$; $^{****}p < 0.0001$.

Please cite this article in press as: Moon et al., Transcriptional intermediary factor 1 gamma prevents lung inflammation and fibrosis via AT2 cells, fibroblasts, and macrophages, Molecular Therapy (2025), https://doi.org/10.1016/j.ymthe.2025.08.035

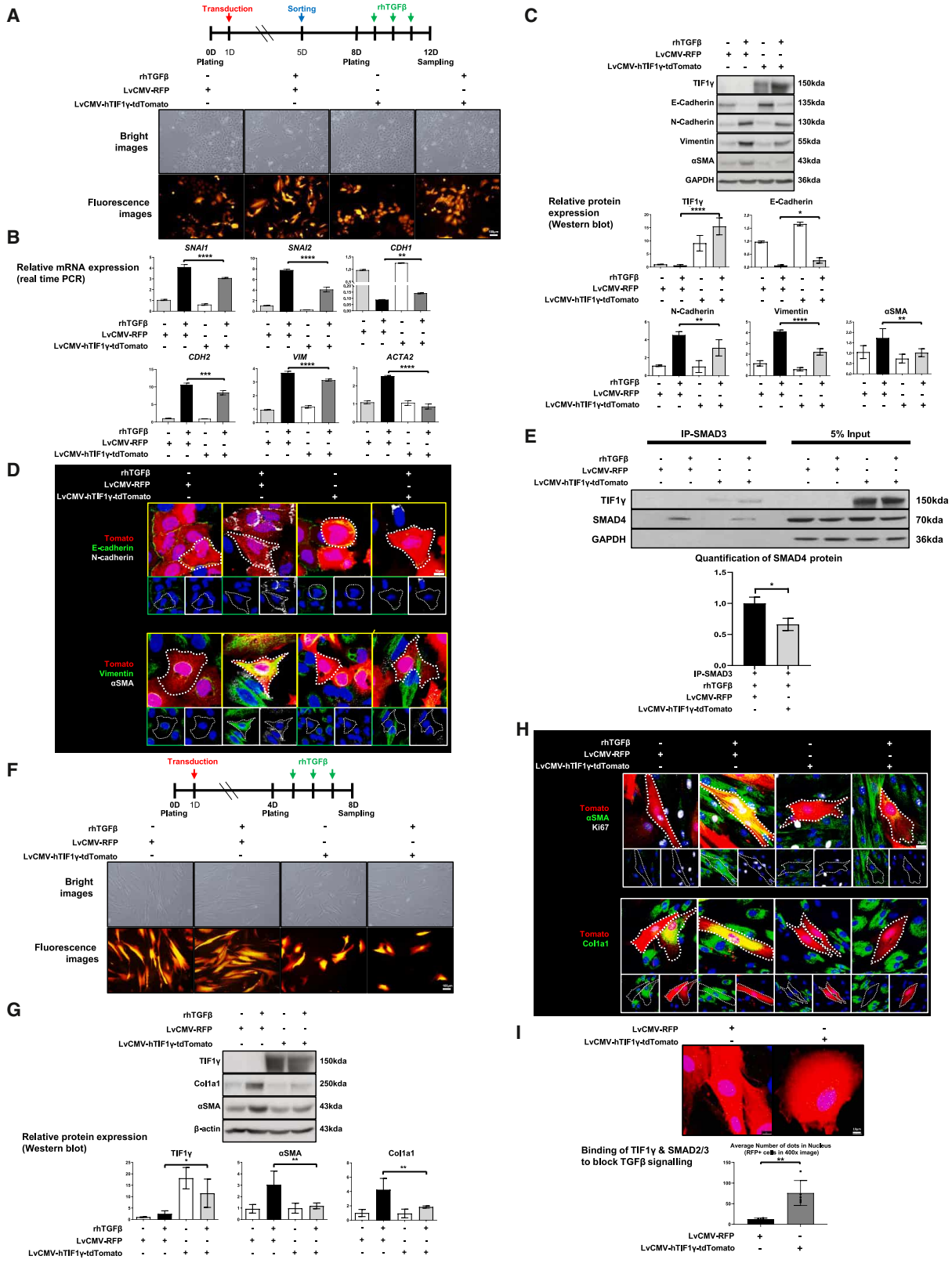

(legend on next page)

Please cite this article in press as: Moon et al., Transcriptional intermediary factor 1 gamma prevents lung inflammation and fibrosis via AT2 cells, fibroblasts, and macrophages, Molecular Therapy (2025), https://doi.org/10.1016/j.ymthe.2025.08.035

TIF1-γ gene transfer (Figures 2H, S1B, and S1C). The inhibitory effect of TIF1-γ on TGF-β signaling in fibroblasts was also supported by the PLA between TIF1-γ and SMAD2/3 (Figure 2I). Therefore, TIF1-γ inhibits fibrosis progression by blocking the TGF-β pathway, thereby preventing EMT in AT2 cells and FMT in fibroblasts.

LipoDo is an effective drug delivery system of plasmid DNA into the damaged fibrotic lung

Before conducting animal experiments, plasmid DNA (pDNA) was chosen as the vector for gene delivery, and lipid nanoparticles (LNPs) were chosen as the drug delivery system (DDS).[12] LNPs provide superior safety benefits to viral vectors, often raising concerns regarding genomic integration and potential long-term, life-threatening adverse effects.[17] For *in vivo* application, we formulated LNPs using DOTAP, a cationic lipid DC-6-14 substitute, which we named LipoDo (DOTAP:DOPE:cholesterol = 4:3:3). DOTAP is a clinically acceptable cationic lipid known for its potent gene delivery properties and effectiveness in lung delivery.[18,19] The characteristics of LipoDo were analyzed by measuring its size, polydispersity index (PDI), zeta potential, and encapsulation efficacy. Particle dispersion and concentration, assessed by turbidity and transmission electron microscopy, confirmed the stable structure of LipoDo (Figures 3A–3C).

In vitro transfection efficiency of LipoDo was tested in 293T cells (Figure 3D) and compared with that of Lipofectamine 2000 (*in vitro* transfection reagent). The efficiency of Lipofectamine 2000 was stable and high regardless of DNA dose. LipoDo exhibited lower transfection efficiency compared to Lipofectamine 2000. However, its efficiency improved at a pDNA concentration of 4 μg compared to 2 μg, although no significant increase was observed at 8 μg. These results suggest the potential for further improvement in transfection efficiency through optimization of the experimental conditions.

Subsequently, the delivery efficiency of LipoDo to the lungs was evaluated in a bleomycin-induced mouse model of PF. On day 7 post-bleomycin treatment, LipoDo containing pDNA was administered systemically into the right ventricular cavity via intracardiac (IC) injection, and organ-specific gene delivery efficiency was assessed. Organ distribution was confirmed by labeling LipoDo with 1,1′-dioctadecyl-3,3,3′,3′-tetramethylindotricarbocyanine iodide (DiR) and monitoring gene expression using CMV promoter-driven luciferase. Under normal conditions without bleomycin, LipoDo injected into the right ventricular cavity primarily accumulated in the liver, spleen, and lungs. However, under the situation of bleomycin-induced PF, LipoDo predominantly accumulated in the lungs, indicating its potential as an effective DDS to the lungs of patients with PF. This enhanced lung accumulation is likely due to increased capillary pressure and structural remodeling in fibrotic lungs, along with the fact that the lung is the first-pass organ following systemic injection via the right ventricle.[20] We next assessed endocytosis and endosomal escape, which are critical indicators DDS performance, and detected luciferase activity in the lungs and spleen, indicating successful gene delivery and transgene expression (Figure 3E). The transfection efficacy of LipoDo in the lungs was evaluated via IC injection of LipoDo + pCMV-green fluorescent protein (GFP) into bleomycin-treated mice. Lung samples collected on day 9 were dissociated into single cells, and GFP^+ cells were analyzed using flow cytometry. Approximately 4%–5% of cells, including AT2 (GFP^+/SPC^+) cells and fibroblasts (GFP^+/$vimentin^+$), were successfully transfected with pDNA (Figure 3F).

TIF1-γ gene therapy effectively alleviates fibrosis in a mouse model of bleomycin-induced PF

Using the validated DDS, we evaluated the anti-fibrotic effect of TIF1-γ in a bleomycin-induced mouse model of PF. This model mimics human PF and was created via intratracheal (IT) instillation of bleomycin that was administered using a catheter to ensure uniform distribution across the lung lobes (Figure S2A). Histological examination at 7 and 14 days post-treatment revealed bilateral fibrosis induction (Figure S2B). To validate the anti-fibrotic effect of TIF1-γ, we administered pCMV-TIF1-γ with LipoDo via IC injection (once on day 7 or twice on days 7 and 9) or via IT instillation (once on day 7 or twice on days 7 and 9) and assessed the lung fibrosis levels on day 20. We quantitated the entire lung fibrosis using micro-computed tomography (microCT) and found a significant reduction of fibrosis in the TIF1-γ-treated group, which was confirmed histologically via hematoxylin and eosin (H&E) staining and Masson's trichrome (MT) staining (Figures 4A and S2C–S2E). TIF1-γ therapy improved lung compliance, indicating reduced lung fibrosis and increased lung parenchyma softness (Figure 4B). Western blotting and qPCR analyses

Figure 2. Evaluation of anti-activation effectiveness and mechanism of TIF1-γ by cell type

(A) Experimental design to evaluate the anti-fibrotic effect of TIF1-γ in human AT2 cells using the human lung adenocarcinoma epithelial cells, A549 cell line. Lentiviruses (CMV-RFP, CMV-TIF1-γ-IRES-tdTomato/MOI 10) are used to introduce genetic modifications, and $tomato^+$ cells are sorted and activated with transforming growth factor β (TGF-β) (10 ng/mL). (B) Quantitative polymerase chain reaction (qPCR) analysis shows upregulation of the epithelial-mesenchymal transition (EMT) and activation markers (including *SNAI1*, *SNAI2*, *CDH2*, *VIM*, and *ACTA2*) by TGF-β and their inhibition by TIF1-γ. TIF1-γ also suppresses the decrease in *CDH1* expression induced by TGF-β. (C) Western blot analysis confirms that TIF1-γ inhibits TGF-β-induced EMT and activation at the protein level in A549 cells. (D) IF images showing that TIF1-γ--transduced AT2 cells maintain E-cadherin expression, inhibit N-cadherin expression, and retain cobblestone-like morphology after TGF-β treatment. TGF-β treatment reduces the expression of mesenchymal marker vimentin and myofibroblast marker αSMA in TIF1-γ-transduced cells. (E) Co-immunoprecipitation shows that TIF1-γ binding to SMAD3 reduces the interaction between SMAD3 and SMAD4 under TGF-β stimulation in A549 cells. (F) Fluorescence microscopy images of human dermal fibroblasts (HDFs) treated with TGF-β showing elongated morphology due to differentiation into myofibroblasts. HDFs transduced with TIF1-γ maintained a rounded morphology. (G) Western blot analysis shows that TIF1-γ inhibited the expression of activation marker αSMA and collagen type 1α1 (Col1a1) at the protein level in HDFs. (H) IF images showing that TIF1-γ-transduced HDFs exhibit suppressed expression of αSMA, Col1a1, and Ki67 and maintain a non-elongated morphology after TGF-β treatment. (I) PLA demonstrating that TIF1-γ binds to SMAD2/3 to block TGF-β signaling in HDFs. Data are presented as mean ± SD. $^*p < 0.05$; $^{**}p < 0.01$; $^{***}p < 0.001$; $^{****}p < 0.0001$.

Please cite this article in press as: Moon et al., Transcriptional intermediary factor 1 gamma prevents lung inflammation and fibrosis via AT2 cells, fibroblasts, and macrophages, Molecular Therapy (2025), https://doi.org/10.1016/j.ymthe.2025.08.035

A

DOTAP: DOPE: Cholesterol = 4: 3: 3

	Size (nm)	PDI	Zeta potential (mV)	Encapsulation efficacy (%)
LipoDo only	109.5±13.34	0.23±0.02	47.01±5.33 (+)	x
LipoDo+pDNA	179.7±14.13	0.15±0.02	35.7±3.67 (+)	94±3

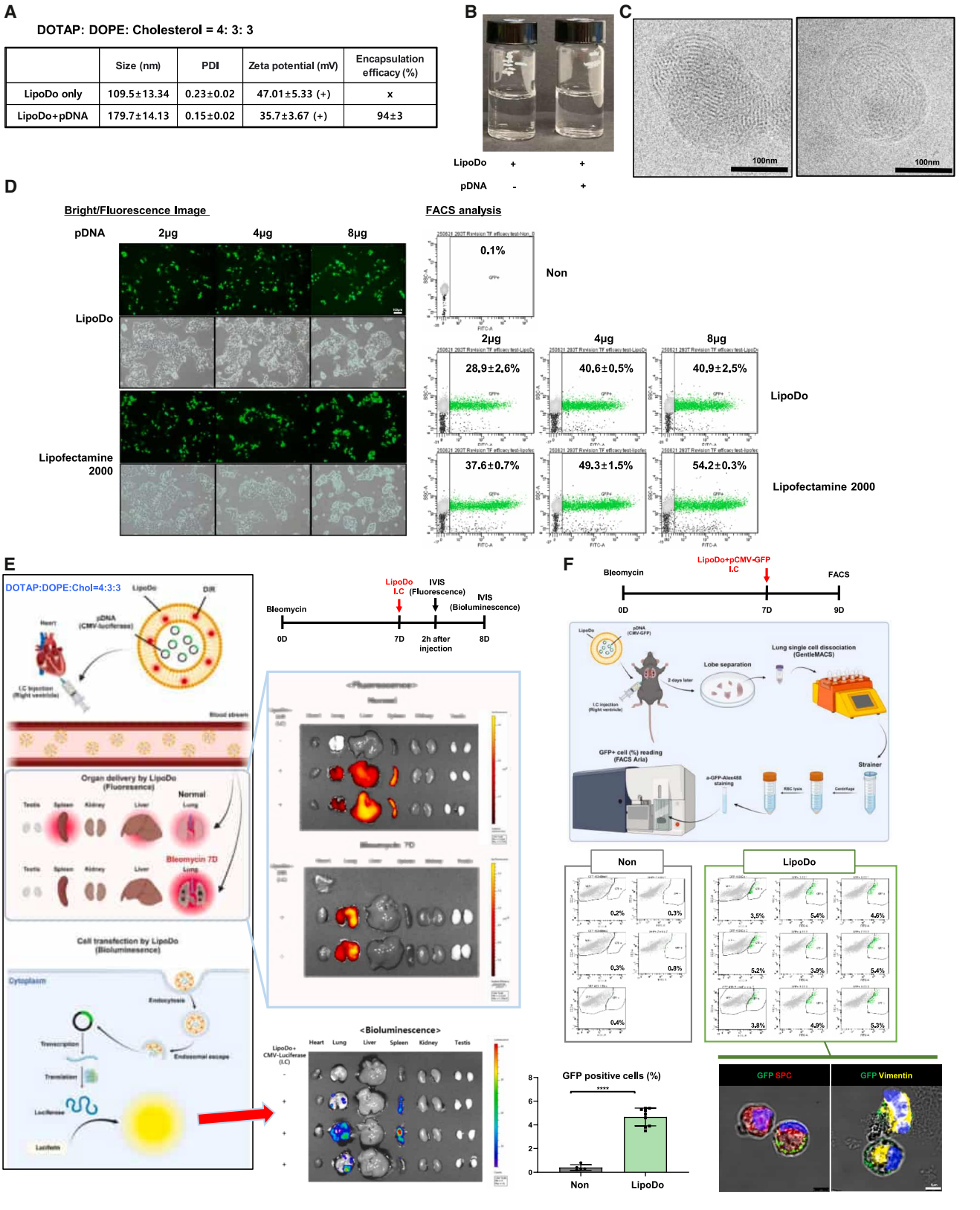

(legend on next page)

Please cite this article in press as: Moon et al., Transcriptional intermediary factor 1 gamma prevents lung inflammation and fibrosis via AT2 cells, fibroblasts, and macrophages, Molecular Therapy (2025), https://doi.org/10.1016/j.ymthe.2025.08.035

of whole-lung tissues revealed reductions in fibrotic markers following TIF1-γ treatment (Figures 4C and 4D). IF analysis of dissociated cells from bleomycin-induced fibrotic lungs in mice demonstrated that TIF1-γ expression reduced fibrotic markers, including vimentin and αSMA, in AT2 cells (Figure 4E). The TIF1-γ treatment improved all indicators of fibrosis pathology, including the Ashcroft score, collagen fiber-occupied alveolar region (%), number of inflammatory cells per unit area (100×), and TGF-β intensity (Figure 4F). These results confirm that TIF1-γ effectively alleviates fibrosis in the mouse model of PF.

TIF1-γ gene therapy inhibits macrophages and reduces cytokines in a mouse model of bleomycin-induced PF

Following the observed decrease in inflammatory cell numbers by TIF1-γ in the previous histological analysis of bleomycin-induced PF in mice (Figure 4F), we quantified this by analyzing the bronchoalveolar lavage fluid (BALF). We observed a significant reduction in inflammatory cell counts and cytokines in the BALF of the TIF1-γ-treated group (Figures 5A and 5B). When we analyzed the cells in BALF from the bleomycin-induced fibrotic lung, we found foam-like activated macrophages, which were decreased in the TIF1-γ-treated group (Figure 5C). Then, we analyzed the subtypes of macrophages from the lung, alveolar macrophages (AMs) double positive for CD170 and F4/80, and interstitial macrophages (IMs) single positive for F4/80 (Figure 5D), and quantitatively assessed them by dissociating the whole lung into single cells, followed by flow cytometry analysis. AMs and IMs were discriminated based on CD170 (SiglecF) expression in flow cytometry analysis. AMs were classified as $CD45^+$, $Ly6G^-$, and $SiglecF^+$. IMs were identified as $CD45^+$, $Ly6G^-$, $SiglecF^-$, and $F4/80^+$. Sequentially, M1 macrophages were defined as $CD45^+$, $Ly6G^-$, $SiglecF^-$, $F4/80^+$, and $MHC2^+$, while M2 macrophages were defined as $CD45^+$, $Ly6G^-$, $SiglecF^-$, $F4/80^+$, and $MHC2^-$. AM decreased by bleomycin, which was not changed by TIF1-γ, whereas IM increased by bleomycin, which was significantly reversed by TIF1-γ (Figure 5E). These findings suggest that TIF1-γ treatment effectively reduces inflammation accompanying PF.

To investigate the anti-inflammatory mechanism of TIF1-γ, we conducted experiments using THP1 cells. After lentivirus transduction (CMV-RFP, CMV-TIF1-γ-tdTomato) and treatment with phorbol 12-myristate 13-acetate (PMA) for differentiation of THP1 cells into macrophages, cells were stimulated with LPS (Figure 5F).

Subsequently, we evaluated the expression levels of inflammatory cytokines (tumor necrosis factor α [TNF-α] and interleukin-1β [IL-1β]). TIF1-γ treatment reduced LPS-induced cytokine expression, as confirmed by qPCR and western blot in cell lysates and by multiplex analysis in cell supernatants (Figures 5G, 5H, and S3A). We investigated the nuclear factor κB (NF-κB) and mitogen-activated protein kinase (MAPK) signaling pathways, both of which are critical regulators of inflammatory cytokine production in macrophages. Treatment of THP1 cells with TIF1-γ resulted in reduced phosphorylation of p65, p38, ERK, and JNK, indicating the inhibition of both NF-κB and MAPK signaling pathways (Figure 5I). These findings suggest that TIF1-γ gene therapy mitigates inflammation during the pathogenesis of bleomycin-induced PF by suppressing NF-κB and MAPK signaling, thereby reducing the secretion of inflammatory cytokines from macrophages.

Evaluation of the anti-fibrotic effects of TIF1-γ using *ex vivo* mouse and human PCLS models

PCLSs were utilized to validate the mechanism and efficacy of TIF1-γ in a model closely mimicking disease conditions.[21,22] Similar to the *in vivo* model, bleomycin-induced mice lung samples were collected after 7 days and embedded in 1.5% low-melting agarose. Serial PCLSs were transduced with TIF1-γ using adenovirus (CMV-GFP or CMV-TIF1-γ-tdTomato). TIF1-γ expression was confirmed via fluorescence on day 2 post-transduction, and samples were stimulated with mouse recombinant TGF-β for another 2 days before sampling (Figure 6A). In a histological analysis, TGF-β treatment induced fibrosis of lung slices, which was effectively inhibited by TIF1-γ-gene transduction (Figure 6B). In IF staining of lung slices, key players such as AT2, fibroblasts, and myofibroblasts showed a different phenotype depending on control or TIF1-γ gene transduction. TIF1-γ transduction inhibited EMT in AT2 cells, FMT in fibroblasts, and collagen secretion in myofibroblasts (Figure 6C). PCLSs from patients with PF (Table S2) were used to evaluate the anti-fibrotic and anti-inflammatory effects of TIF1-γ in clinical settings. Human lung tissue from patients undergoing lung transplantation surgery was infused with 1.5% low-melting agarose, solidified with cold phosphate-buffered saline (PBS), and embedded. Serial PCLSs were then cultured and transduced with TIF1-γ or control GFP gene using an adenovirus. Expression of the transduced genes in PCLSs viable in culture dishes was confirmed via fluorescence on day 2 post-transduction. To investigate the anti-fibrotic and anti-inflammatory effect of TIF1-γ in human PCLSs, the samples were stimulated with TGF-β for 3 days and LPS for 2 days, respectively (Figures 6D and S4A). Fluorescence imaging confirmed similar transduction efficiency for both adenoviral vectors (CMV-GFP or CMV-TIF1-γ-tdTomato) and showed that TIF1-γ introduction attenuated fibrosis (Figure 6E). Histological analysis revealed that TGF-β treatment for 3 days induced fibrosis in human lung slices, which was significantly reduced by TIF1-γ gene transduction (Figure 6F). In the western blot analysis, induction of fibrotic

Figure 3. LipoDo is an effective drug delivery system for delivering plasmid DNA to the lungs in a mouse model of bleomycin-induced PF

(A) Characteristics of LipoDo (including size, polydispersity index [PDI], zeta potential, and encapsulation efficacy). (B) Turbidity of LipoDo in water. (C) Cryogenic electron microscopy image of LipoDo construct. (D) Transfection ability tests are conducted using LipoDo and Lipofectamine 2000 in 293T cells. Transfection efficiency is confirmed via flow cytometry and western blot analysis. (E) The organ distribution of LipoDo is assessed using IVIS. (F) The transfection efficacy of LipoDo+pCMV-GFP in mouse lungs is analyzed using flow cytometry. SPC used for AT2 and vimentin used for fibroblast cells. IC, intracardiac injection. Data are presented as mean ± SD. $^*p < 0.05$, $^{**}p < 0.01$, $^{***}p < 0.001$, and $^{****}p < 0.0001$.

Please cite this article in press as: Moon et al., Transcriptional intermediary factor 1 gamma prevents lung inflammation and fibrosis via AT2 cells, fibroblasts, and macrophages, Molecular Therapy (2025), https://doi.org/10.1016/j.ymthe.2025.08.035

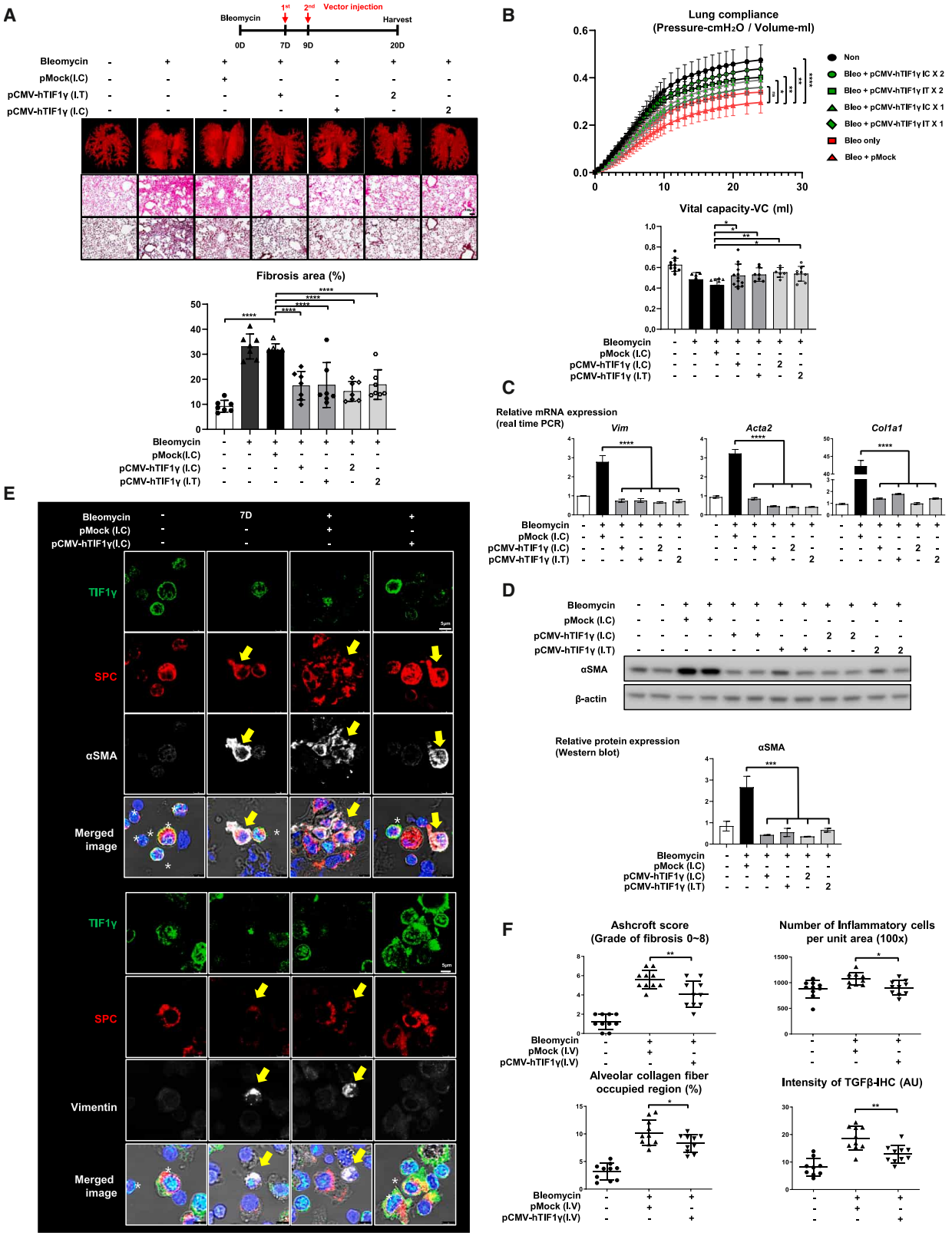

(legend on next page)

Please cite this article in press as: Moon et al., Transcriptional intermediary factor 1 gamma prevents lung inflammation and fibrosis via AT2 cells, fibroblasts, and macrophages, Molecular Therapy (2025), https://doi.org/10.1016/j.ymthe.2025.08.035

markers by TGF-β was effectively blocked by TIF1-γ gene therapy (Figure 6G). IF staining confirmed that TIF1-γ inhibited EMT in AT2 cells and FMT in fibroblasts, consistent with *ex vivo* results using human PCLSs (Figure 6H). In multiplex assays, LPS treatment for 2 days as an inflammatory stimulus significantly reduced IL-1β and TNF-α levels in the cell supernatant in the TIF1-γ group. Additionally, transduced fluorescent cells remaining adhered to the bottom of the culture plate displayed a macrophage-like morphology (Figure 6I). Notably, cells detached from the PCLSs and macrophages within the PCLS tissue showed reduced TNF-α and IL-1β expression after TIF1-γ gene transduction (Figures 6J and S4B). The anti-fibrotic effects of TIF1-γ are confirmed by the *ex vivo* cultures mimicking early fibrosis having inflammatory conditions in both mouse and human models.

DISCUSSION

Current therapies for PF are limited by the high rate of refractory cases and insufficient efficacy, often only slowing disease progression. Since lung fibrosis is a highly dynamic and complex process,[23] multiple treatment strategies that target the cells and signaling pathways essential to PF pathogenesis are needed.[24] Here, we investigated the potential of TIF1-γ as a gene therapy for PF by targeting key signaling pathways involved in disease progression. The antifibrotic mechanisms of TIF1-γ were elucidated in three key cell types contributing to PF: AT2 cells, fibroblasts, and macrophages. In AT2 cells, TIF1-γ was shown to block TGF-β-induced EMT. In fibroblasts, TIF1-γ inhibited FMT, and in macrophages, it suppressed activation. These findings demonstrate that TIF1-γ can systematically inhibit fibrosis by targeting major cell types involved in PF. This represents a significant distinction from previous studies, which primarily focused on the role of TIF1-γ in hepatic fibrosis by investigating its effects on HSCs. These results also highlight the potential for expanding the scope of the role of TIF1-γ in anti-fibrotic therapy.

Additionally, we developed an optimized DDS, LipoDo, that ensured efficient delivery of the TIF1-γ gene to the fibrosis-stimulated lungs after systemic or IT administration, leading to a significant prevention of fibrosis in a bleomycin-induced mouse model of PF. Because the lung is the first-pass organ after both intravenous (IV) and IC-right ventricular injection, nanoparticles inevitably encounter the pulmonary capillary bed first; in the bleomycin-induced fibrosis model, capillary narrowing and elevated vascular pressure further favor their entrapment in the lung parenchyma, explaining the strong lung tropism of LipoDo.

Despite the significant progress in elucidating the pathophysiology of PF, a translational gap remains between bench and bedside or between animal and human data. Thus, transformative experimental strategies are required for developing the effective anti-fibrotic therapies.[25] To assess the clinical applicability of TIF1-γ for human fibrotic disease, we used PCLSs from surgical lung specimens of patients with PF to evaluate the anti-fibrotic effects of TIF1-γ in a model that closely mimics human clinical trials. Confirmation of the therapeutic effect of TIF1-γ in the viable human lung tissue suggests that the anti-fibrotic mechanisms of TIF1-γ observed *in vitro* and in animal models can be translated to patients, providing compelling evidence that TIF1-γ can be a viable therapeutic option for PF.

While these results are promising, this study has some limitations. First, although LipoDo showed efficient gene delivery to fibrotic lungs, further optimization of delivery efficacy is needed. When bleomycin-induced PF was treated on day 7 via IT instillation, the vector did not disperse well owing to severe bronchial damage by bleomycin, leading to deaths. Regarding clinical applicability, IT administration is more widely used than the IV route for PF. Therefore, improving the formulation of LipoDo + pDNA to an inhalable form or switching to a viral vector with higher lung delivery efficiency could overcome the practical hurdle and guarantee therapeutic efficacy. Second, CMV promoters enhance constitutive and ubiquitous gene expression. It is an optimal strategy for treating genetic disorders. However, off-target effects, which lead to unexpected events, considerably limit treating certain diseases.[26,27] To control the expression of therapeutic genes based on specific pathologic conditions in specific target cells or organs, a strategy to select a promoter in front of the therapeutic gene is required. Therefore, a TGF-β promoter-driven construct is considered feasible for inducing TIF1-γ expression in the inflamed lungs undergoing fibrosis.

The next step is to prepare for clinical trials of TIF1-γ gene therapy. Development of Good Manufacturing Practice (GMP) for pDNA + LipoDo from GMP production of plasmid is under way.

In conclusion, our study provides strong evidence that TIF1-γ is a candidate gene therapy for PF. It effectively inhibits TGF-β

Figure 4. Treatment with TIF1-γ effectively alleviates fibrosis in a mouse model of bleomycin-induced PF

(A) Representative images of micro-computed tomography, hematoxylin and eosin (H&E), and MT slides from each group alongside quantitative data on fibrosis area measured using micro-computed tomography. (B) Pulmonary function test analysis (pressure-volume loop-lung compliance and vital capacity). (C) Verification of fibrotic marker mRNA expression levels in the whole lung using qPCR. (D) Verification of α-smooth muscle actin (αSMA) protein expression levels in the whole lung using western blot analysis. (E) IF staining of cytospin lung cells dissociated from whole-lung tissue, showing TIF1-γ (green), SPC (red), and αSMA or vimentin (white). Yellow arrows indicate activated AT2 cells ($SPC^+/\alpha SMA^+$ or $vimentin^+/TIF1\text{-}\gamma^-$), and asterisks (*) indicate non-activated AT2 cells ($SPC^+/TIF1\text{-}\gamma^+/\alpha SMA^-$ or $vimentin^-$). IC and IT are intracardiac and intratracheal administration, respectively. (F) Histological assessment of lung fibrosis in mice treated with LipoDo/pCMV-TIF1-γ via tail vein injection (intravenous [IV]), independently conducted by a contract research organization ($N = 10$). Fibrotic changes were quantified using four histological indicators: Ashcroft score, number of infiltrated inflammatory cells (H&E staining), alveolar collagen fiber-occupied region (MT staining), and TGF-β expression (immunohistochemistry). Data are presented as mean ± SD. $^*p < 0.05$; $^{**}p < 0.01$; $^{***}p < 0.001$; $^{****}p < 0.0001$.

Please cite this article in press as: Moon et al., Transcriptional intermediary factor 1 gamma prevents lung inflammation and fibrosis via AT2 cells, fibroblasts, and macrophages, Molecular Therapy (2025), https://doi.org/10.1016/j.ymthe.2025.08.035

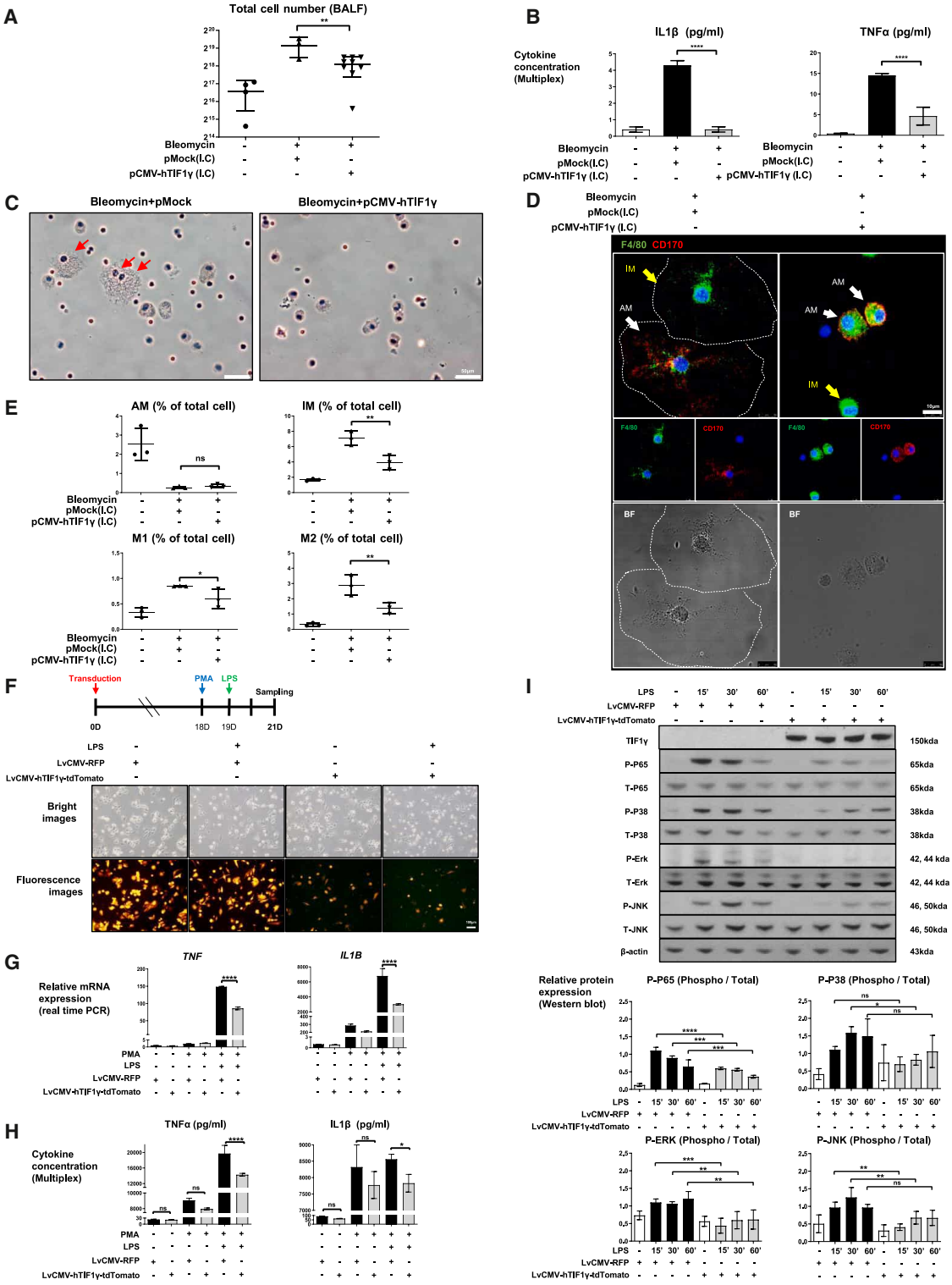

Figure 5. Treatment with TIF1-γ alleviates the progression of PF by reducing the secretion of inflammatory cytokines by macrophages

(A) The total number of cells in bronchoalveolar lavage fluid (BALF) was quantified. (B) Inflammatory cytokines (including interleukin 1β [IL-1β] and tumor necrosis factor alpha [TNF-α]) in BALF were assessed using multiplex analysis. (C) BALF cells are subjected to cytospin and stained with H&E. Red arrow indicates activated macrophage. (D) BALF cells were subjected to cytospin and IF staining targeting F4/80 (pan macrophage marker) and CD170 (alveolar macrophage [AM] marker). The yellow arrow indicates

(legend continued on next page)

signaling and inflammation by modulating cells essentially involved in PF, such as AT2 cells, fibroblasts, and macrophages. Reproducible efficacy of TIF1-γ in the viable human lung tissues demonstrates its promising potential as a gene therapeutic for patients with PF.

MATERIALS AND METHODS

Human GEO data

Collection of scRNA-seq data on the human lungs

We collected published scRNA-seq data from the human lungs. The data deposited in the GEO were downloaded (GSE135893). The data originally consisted of 30 datasets; however, only 22 samples were selected, comprising 10 control samples and 12 idiopathic PF samples. All data were deposited in the form of Cell Ranger (10× Genomics) count matrices.

Data processing

All data were processed using the Cell Ranger count pipeline (version 3.0.2) with the GRCh38 human genome reference. The pipeline generated gene expression matrices, estimating 170,375 cells from 22 samples. For quality control, matrices were imported into R and processed using the Seurat package (version 4.3.0). Cells were retained if they met the following criteria: mitochondrial transcript percentage <25%, unique molecular identifier count $\leq$50,000, and expressed gene count between 200 and 7,500, resulting in 123,136 cells for further analysis. After quality control, data were normalized using the SCTransform function. Batch effects were adjusted by integrating the datasets using SelectIntegrationFeatures, PrepSCTIntegration, FindIntegrationAnchors, and IntegrationData. The number of principal components for clustering was determined using RunPCA. Clustering and projection onto uniform manifold approximation and projection (UMAP) were performed with FindNeighbors, FindClusters, and RunUMAP. For downstream analysis, differentially expressed genes were identified using the FindMarkers function, calculating average log2 fold change and statistical significance. Gene expression levels were visualized with FeaturePlot and VlnPlot functions in Seurat.

A549 culture

The human lung epithelial cell line A549 was purchased from the Korean Cell Line Bank (catalog no. 10185). A549 cells were cultured in RPMI 1640 (catalog no. 11875093, Gibco) supplemented with 10% fetal bovine serum (FBS; catalog no. F0900-050, GenDEPOT) and 1% (v/v) penicillin/streptomycin (P/S; catalog no. 15070063, Gibco) in a humidified incubator with 5% CO_2. To validate the anti-EMT effect of optiTIF1-γ in AT2 pneumocytes, the cells were transduced with lentivirus (purchased from VectorBuilder). Tomato$^+$ cells were sorted using fluorescence-activated cell sorting (FACS), plated, and treated daily with 10 ng/mL recombinant human (rh)TGF-β (catalog no. 7754-BH-005, R&D Systems) for 3 days.

THP1 culture

The human monocyte cell line THP1 was purchased from the American Type Culture Collection (catalog no. TIB-202). THP1 cells were cultured in RPMI 1640 (catalog no. A1049101, Gibco) with 10% FBS (catalog no. F0900-050; GenDEPOT) and 1% (v/v) P/S (catalog no. 15070063; Gibco). THP1 cells were cultured in a humidified incubator with 5% CO_2. To validate the anti-activation effect of optiTIF1-γ in macrophages, THP1 cells were transduced with lentivirus (purchased from VectorBuilder). PMA (catalog no. P8139, Sigma) at 10 ng/mL was added to induce differentiation into macrophages. After 1 day, 100 ng/mL LPS (catalog no. L3129, Sigma) was added for activation, and sampling was conducted 2 days later.

HDF culture

The HDF cell line was purchased from Thermo Fisher Scientific (catalog no. C0135C). HDF cells were cultured in DMEM (catalog no. 11995065, Gibco) with 10% FBS (catalog no. F0900-050, GenDEPOT), 1% L-glutamine (catalog no. 25030081, Gibco), and 1% (v/v) P/S (catalog no. 15070063, Gibco). HDF cells were cultured in a humidified incubator with 5% CO_2. To validate the anti-FMT effect of optiTIF1-γ in fibroblasts, the cells were transduced with lentivirus (purchased from VectorBuilder). After confirming the expression of optiTIF1-γ using tomato, 10 ng/mL rhTGF-β (catalog no. 7754-BH-005, R&D Systems) was administered daily for 3 days.

PLA

The cells (A549, HDF, and THP1) were plated on confocal dishes (catalog no. 801002, NEST), washed with PBS, and fixed with 4% paraformaldehyde (PFA; catalog no. 163-20145, Wako) for 15 min. After washing with PBS, the cells were permeabilized with a buffer (0.5% TX-100 in PBS) at room temperature (RT) for 15 min. A blocking solution (Duolink kit, catalog no. DUO92106, Sigma) was applied at 37°C for 1 h. The cells were then incubated overnight at 4°C with primary antibodies (TIF1-γ-Rb/SMAD2/3-Gt). Staining was performed using the Duolink *In Situ* Starter Kit Goat/Rabbit (catalog no. DUO92106, Sigma) and Duolink *In Situ* Detection Reagent Green (catalog no. DUO92014, Sigma) according to the manufacturer's instructions. Images were obtained using a Leica confocal microscope (TCS SP8). To confirm the interaction between TIF1-γ and SMAD2/3, the number of dots in the nucleus of tomato$^+$ cells was measured using LAS-X software.

interstitial macrophages (IMs), whereas the white arrow indicates AMs. (E) Following single-cell dissociation of the entire lung, flow cytometry is performed to identify macrophage subtypes. (F) THP1 cells (human monocyte cell line) are transduced with lentivirus (CMV-RFP or CMV-hTIF1-γ-tdTomato), differentiated into macrophages with phorbol 12-myristate 13-acetate (PMA) treatment, and then exposed to lipopolysaccharide (LPS) for 2 days before sampling. (G) mRNA expression levels of inflammatory cytokines (*TNF* and *IL1B*) are determined via qPCR. (H) The level of inflammatory cytokines (TNF-α and IL-1β) secreted into the cell supernatant is quantified using multiplex analysis. (I) Western blotting analysis is conducted to assess the NF-κB (P65) and MAPK (P38, ERK, and JNK) signaling pathways, upstream regulators of inflammatory cytokines. Data are presented as mean ± SD. *$p < 0.05$; **$p < 0.01$; ***$p < 0.001$; ****$p < 0.0001$.

Please cite this article in press as: Moon et al., Transcriptional intermediary factor 1 gamma prevents lung inflammation and fibrosis via AT2 cells, fibroblasts, and macrophages, Molecular Therapy (2025), https://doi.org/10.1016/j.ymthe.2025.08.035

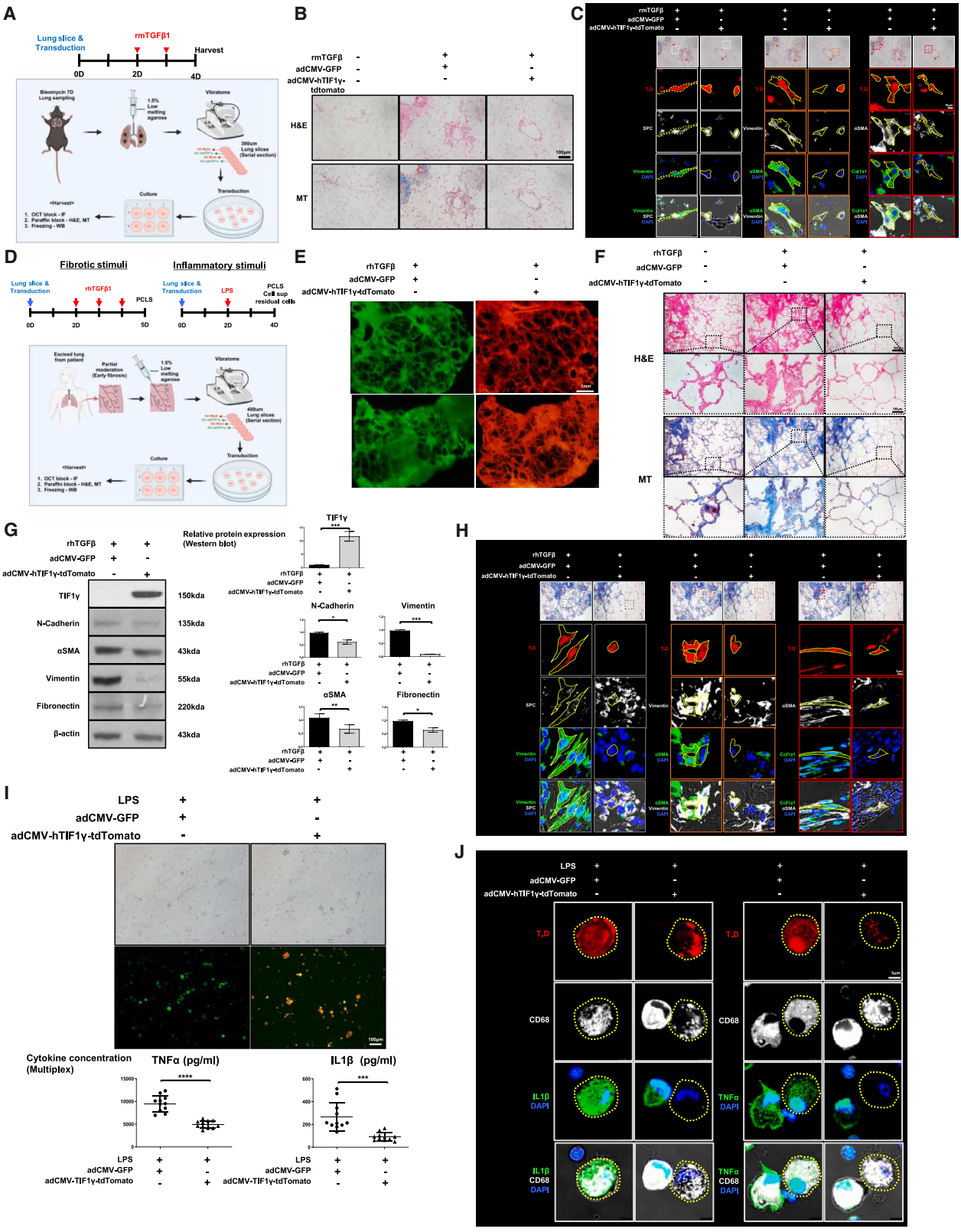

(legend on next page)

Preparation of liposome-LipoDo

Production of LipoDo

Three liposome components (DOTAP [catalog no. 890890P, Avanti], DOPE [catalog no. 850725P, Avanti], cholesterol [catalog no. 700000P, Avanti]) were dissolved in *tert*-butanol (catalog no. 471712, Sigma). DOTAP, DOPE, and cholesterol were mixed in a ratio of 10:7.5:7.5 μmol, followed by the addition of *tert*-butanol four times the volume of the mixture. The mixture was then frozen at −80°C for over 4 h and freeze-dried (Alpha 2–4 LSC, Martin Christ) for 2 days to obtain a lipid cake. Ultrapure distilled water (catalog no. 10977015, Invitrogen), 1 mL, was added to the lipid cake, and the mixture was vortexed for 10 min (10 mM stock-DOTAP standard). The mixture was vortexed every 30 min at 37°C in an ultrasonic bath (Branson 5800) and sonicated for 2 h. It was then allowed to rest for at least 2 h at 4°C before use.

Packaging plasmid in LipoDo

LipoDo (140 nmol) and plasmid (18 μg) were briefly vortexed and incubated for 20 min at 25°C. The solution was transferred to a Vivaspin2 concentrator (catalog no. VS0252, VIVASCIENCE) and centrifuged three times at 1,500 × *g* for 5 min at 25°C. The upper part of the column was then reversed, and its contents were centrifuged at 3,000 × *g* for 3 min at 25°C. The volume was adjusted to 50 μL for IC injection and 20 μL for IT instillation.

Animal model

All animal experiments were conducted according to the ARRIVE (Animal Research: Reporting of *In Vivo* Experiments) guidelines. All *in vivo* studies were approved by the Institutional Animal Care and Use Committee (no. 22-0308-S1A0) of Seoul National University Hospital (Seoul, Republic of Korea). C57BL/6 mice (20–25 g, male, 10 weeks old) were used for the experiments. To induce PF, bleomycin (catalog no. B1141000, Sigma) was administered at a dose of 1 mg/kg (catalog no. 163678, Sigma-Aldrich) through IT instillation. Using a ventilator (Inspira ASV, Harvard Apparatus) at a rate of 120 BPM with a volume of 0.3 mL for 1 min, bleomycin was uniformly distributed throughout the lungs. Vectors (pVAX1 [backbone] and pCMV-optimized hTIF1-γ) were injected into the mice (18 μg/head) through IC injection or IT instillation.

LipoDo delivery validation *in vivo*

To evaluate liposome delivery efficiency, Liposome (LipoDo)-DiR-tagged and pDNA (CMV-luciferase) were used in mice. PF was induced using bleomycin, and on day 7, the lipo complex was administered. After 2 h, the liver, lungs, kidneys, spleen, and testes were sampled. DiR fluorescence was assessed using an *in vivo* imaging system (IVIS) to determine organ-specific liposome distribution. After 24 h, the same organs were sampled to assess transfection efficiency. The organs were incubated with D-luciferin (catalog no. P1042, Promega) for 15 min and then analyzed using the IVIS system (IVIS Lumina S5, PerkinElmer) to measure bioluminescence, indicating pDNA (CMV-luciferase) expression.

MicroCT

Mouse lungs were perfused with PBS and then excised. The lungs were fixed in a 4% PFA solution (catalog no. 163-20145, Wako). Following fixation, the lungs were incubated for 2 h each in 70%, 80%, and 90% ethanol and then overnight in 100% ethanol for dehydration. The lungs were subsequently incubated in hexamethyldisilazane (catalog no. A15139AP, Sigma) for 2 h and air-dried. The mouse lungs were scanned using a microCT instrument (Quantum GX2, PerkinElmer) with the following settings: 90 kV X-ray voltage, 88 μA current, 57 min scan time, 10 mm field of view, and 20-μm pixel size. Images and quantitative data were obtained using Analyze12 software (PerkinElmer).

Pulmonary function test

A mixture of alfaxan and rumpun was administered to the mouse through intramuscular injection to induce anesthesia. After anesthesia, the mouse was intubated by making an incision in the trachea and inserting a tube. After the surgery, the mouse was positioned on the bed of the pulmonary function test (PFT) device (DSI-Buxco), and PFT was measured following the manual instructions. PFT analysis was performed using the FinePointe software (DSI-Buxco).

BALF sampling

Mouse BALF was collected by lavaging the lungs with 800 μL sterile PBS through the trachea, aspirating the fluid back, and repeating this process three times. The collected BALF was centrifuged at 400 × *g* for 7 min at 4°C, and the supernatant was separated for multiplex analysis of inflammatory cytokines. BALF cells were fixed with

Figure 6. Evaluation of the anti-fibrotic effects of TIF1-γ using *ex vivo* mouse and human precision-cut lung slice (PCLS) models

(A) Mouse PCLS *ex vivo* graphic scheme. (B) Mouse PCLS H&E and MT staining images. (C) The anti-epithelial-mesenchymal transition (EMT) effect of TIF1-γ in AT2 cells (vimentin/SPC), the anti-FMT effect in fibroblasts (αSMA/vimentin), and the reduction in collagen secretion in myofibroblasts (Col1a1/αSMA) are confirmed using mouse PCLS IF. Green indicates the activation marker, red represents the transduced cells, and white denotes the cell marker (pseudo-color). (D) Human PCLS *ex vivo* graphic scheme. (E) Fluorescence microscopy images of human PCLS at sampling time (5 days) (serial section confirm). (F) Human PCLS H&E and MT staining images. (G) Western blot analysis of fibrotic markers (including N-cadherin, αSMA, vimentin, and fibronectin) in human PCLS. (H) The anti-EMT effect of TIF1-γ in AT2 cells (vimentin/SPC), the anti-FMT effect in fibroblasts (αSMA/vimentin), and the reduction in collagen secretion in myofibroblasts are confirmed using human PCLS IF. Green indicates the activation marker, red represents the transduced cells, and white denotes the cell marker (pseudo-color). (I) Fluorescence images of residual cells from human PCLS at sampling time (4 days) observed (transduction and macrophage morphology confirm and inflammatory cytokines TNF-α and IL-1β) in human PCLS supernatant are measured using multiplex analysis. (J) IF of residual cells from human PCLS. CD68 used for macrophage, and TNF-α and IL-1β are stained. Green indicates the activation marker, red represents the transduced cells, and white denotes the cell marker (pseudo-color). Residual cells from the bottom of the culture plate show CD68 positivity, with decreased IL-1β and TNF-α expression. Data are presented as mean ± SD. $^{*}p < 0.05$; $^{**}p < 0.01$; $^{***}p < 0.001$; $^{****}p < 0.0001$.

1 mL 4% PFA on ice for 8 min, then centrifuged at 400 × *g* for 7 min at 4°C to remove the PFA. The cells were resuspended in 3 mL Dulbecco's PBS (DPBS), centrifuged again at 400 × *g* for 7 min at 4°C, and finally resuspended in 500 μL PBS. BALF cells (4×10^4/200 μL) were spun onto slides at 600 rpm for 10 min and processed for H&E staining. BALF cells (1×10^4/200 μL) were spun onto slides at 600 rpm for 10 min and processed for IF staining.

PCLS culture

Mouse

PF was induced by IT instillation of bleomycin (1 mg/kg body weight). On day 7 post-instillation, mice were anesthetized, and lungs were harvested for analysis. To remove blood, the right ventricle of the heart was perfused with PBS at a flow rate of 7 mL/min. Subsequently, 800 μL of 1.5% low-melting agarose (catalog no. 16520-100, Invitrogen) was slowly instilled through the trachea. The lungs were allowed to inflate, and the agarose was solidified using ice. The lungs were then excised, and the left lobe was embedded in 1.5% low-melting agarose gel. The agarose-embedded left lung lobe was sectioned into 300-μm-thick slices using a vibratome (Leica, VT1200s) to obtain serial sections. The PCLSs were infected with adenovirus (CMV-GFP or CMV-hTIF1-γ-tdTomato) by forming droplets containing 1×10^9 viral particles (VP)/150 μL of culture media on each slice. The slices were incubated for 12 h. After incubation, the media was changed to DMEM (catalog no. 11995065, Gibco) containing 10% FBS (catalog no. F0900-050, GenDEPOT) and 1% (v/v) P/S (catalog no. 15070063, Gibco). On day 2 post-infection, transduction efficiency was confirmed using fluorescence microscopy, and the PCLSs were treated with recombinant mouse TGF-β (10 ng/mL). After 2 days of treatment, the slices were harvested for further analysis. The slices intended for optimal cutting temperature compound (OCT) and paraffin embedding were fixed by placing them on slide glasses and adding 500 μL of 4% PFA per slice. A cover glass was placed on top to flatten the slices, which were then fixed for 15 min at RT. After fixation, the slices were washed with PBS and embedded in either OCT or paraffin for further histological analysis.

Human

During lung transplantation at Seoul National University Hospital, the middle lobe of the excised lung was placed in 37°C Hank's balanced salt solution (catalog no. 24020-117) and transported to the laboratory. Using a 50-mL syringe, 50 mL of 1.5% low-melting agarose (catalog no. 16520-100; Invitrogen) was slowly filled into the terminal bronchus. The bronchus was clamped using forceps and immersed in cold PBS for 30 min to solidify the agarose. The agarose-filled section was cut into 2-cm^3 cubes and embedded in 1.5% low-melting agarose. The vibratome (Leica, VT1200s) was used to obtain 400-μm-thick PCLSs in serial sections. The PCLSs were infected with adenovirus (CMV-GFP or CMV-hTIF1-γ-tdTomato) at a concentration of 5×10^9 VP/300 μL culture media per slide in a 48-well plate, followed by incubation for 12 h. After incubation, the media was changed to DMEM with 10% FBS and 1% P/S. On day 2 post-infection, transduction efficiency was confirmed using fluorescence microscopy. The PCLSs were then treated with rhTGF-β (10 ng/mL) and sampled after 3 days. For OCT and paraffin embedding, the slices were placed on slide glasses, and 500 μL of 4% PFA was added per slice. A cover glass was placed on top to flatten the slices, which were then fixed for 15 min at RT. Subsequently, the slices were washed with PBS and embedded in either OCT or paraffin. More than three slices were frozen in liquid nitrogen, ground in a mortar and pestle, and used for western blot analysis. Information about the lung tissue donor is presented in Table S2. This study was approved by the institutional review board (IRB) of Seoul National University Hospital (IRB no. 2308-051-1456).

Antibodies

IF, western blot, and flow cytometry assays

Rabbit polyclonal a-TIF1-γ (custom-made)

Rabbit polyclonal a-TIF1-γ (catalog no. ab84455, Abcam)

Mouse monoclonal a-αSMA (catalog no. A5228, Sigma-Aldrich)

Rabbit polyclonal a-αSMA (catalog no. ab5694, Abcam)

Mouse monoclonal a-αSMA-660 (catalog no. 50-9760-82, Thermo Fisher Scientific)

Mouse monoclonal a-N-cadherin (catalog no. sc-59987, Santa Cruz Biotechnology)

Rabbit monoclonal a-E-cadherin (catalog no. sc-59987, Santa Cruz Biotechnology)

Rabbit polyclonal a-collagen I (catalog no. PA5-29569, Invitrogen)

Mouse a-fibronectin (catalog no. sc-18825, Santa Cruz Biotechnology)

Rabbit monoclonal a-vimentin (catalog no. 5741S, Cell Signaling Technology)

Rat monoclonal a-vimentin (catalog no. MAB2105, R&D Systems)

Mouse a-SPC (catalog no. sc-518029, Santa Cruz Biotechnology)

Rabbit a-SPC-A647 (catalog no. bs-10067R-A647, Bioss)

Rabbit a-SPC-A488 (catalog no. bs-10067R-A488, Bioss)

Rabbit a-TGF-β (catalog no. ab92486, Abcam)

Mouse monoclonal β-actin (catalog no. sc-47778, Santa Cruz Biotechnology)

Mouse monoclonal a-GAPDH ([glyceraldehyde 3-phosphate dehydrogenase] catalog no. MA5-15738, Thermo Fisher Scientific)

Rabbit polyclonal a-GAPDH (catalog no. Ab9485, Thermo Fisher Scientific)

Rabbit polyclonal a-GFP-488 (catalog no. A21311, Thermo Fisher Scientific)

Rabbit a-F4/80 (catalog no. 30325T, Cell Signaling Technology)

Rat a-F4/80-APC (catalog no. 17-4801-82, eBioscience)

Rat a-CD170 (catalog no. 14-1702-82, eBioscience)

Rabbit a-IL-1β (catalog no. P420B, Thermo Fisher Scientific)

Rabbit a-TNF-α (catalog no. 6945S, Cell Signaling Technology)

Mouse monoclonal a-PCNA (catalog no. MA5-11358, Thermo Fisher Scientific)

Mouse monoclonal a-Ki67 (catalog no. 9449S, Cell Signaling Technology)

Rat monoclonal a-Ly-6C-785 (catalog no. 128041, BioLegend)

Rat monoclonal a-MHCII-PerCP (catalog no. 107624, BioLegend)

Rat monoclonal a-CD45-395 (catalog no. 564279, BD)

Rat monoclonal a-SiglecF-647 (catalog no. 562680, BD)

Mouse monoclonal a-CD64-650 (catalog no. 740622, BD)

Rat monoclonal a-Ly6G-PE (catalog no. 551461, BD)

Rat monoclonal a-F4/80-450 (catalog no. 48-4801-82, Invitrogen)

Rat monoclonal a-CD3-PE-Cy7 (catalog no. 100220, BioLegend)

Rat monoclonal a-CD45R/B220-605 (catalog no. 563708, BD)

Rat monoclonal a-CD206-700 (catalog no. 141734, BioLegend)

Rat monoclonal a-CD11b-APC-Cy7 (catalog no. 101226, BioLegend)

Rabbit monoclonal a-TAK1 (catalog no. 5206S, Cell Signaling Technology)

Rabbit polyclonal a-Phospho-TAK1 (catalog no. 9339S, Cell Signaling Technology)

Rabbit monoclonal a-Phospho-TAK1 (catalog no. 4508S, Cell Signaling Technology)

Rabbit monoclonal a-Phospho-SMAD3 (catalog no. 9520S, Cell Signaling Technology)

Rabbit monoclonal a-SMAD3 (catalog no. 9523S, Cell Signaling Technology)

Mouse monoclonal a-SMAD3 (catalog no. MA5-15663, Thermo Fisher Scientific)

Rabbit monoclonal a-SMAD4 (catalog no. 46535S, Cell Signaling Technology)

Goat polyclonal a-SMAD2/3 (catalog no. Sc-6032, Santa Cruz Biotechnology)

Characterization of LipoDo

To characterize LipoDo, a 1-mM LipoDo + plasmid vector was prepared. The preparation procedures followed the same steps as those described for the preparation of LipoDo with plasmid.

Cryogenic electron microscopy

Morphological examination was conducted using a cryogenic electron microscopy (cryo-EM) system (JEM-1400, JEOL). To prepare samples for cryo-EM imaging, 300 mesh copper grids coated with lacey carbon from Electron Microscopy Sciences were glow discharged prior to use. Four microliters of the sample solution was applied to the grid in a 100% humidity environment, blotted with filter paper for 2 s with no applied blot force, and rapidly plunged into liquid ethane using a Vitrobot (FEI Company). Imaging of the cryo-grids was carried out using a 200-keV field emission gun transmission electron microscope (Arctica, FEI Company) equipped with a Falcon II direct electron detector (FEI Company). Images were taken at a magnification of 53,000× with a 1-s exposure time. Fast Fourier transforms of the images were performed using ImageJ software.

Particle size, PDI, and zeta potential

The particle size and zeta potential were determined using a dynamic light scattering detector (ZetaView, Particle Metrix). Briefly, additional DPBS was added to each sample to make up a total volume of 1 mL. Next, particle size and zeta potential were analyzed using the ZetaView program.

Encapsulation efficacy

The encapsulation efficacy was measured using the PicoGreen assay kit (catalog no. P7589, Thermo Fisher Scientific) according to the manufacturer's instructions. Briefly, the test sample was prepared by mixing 5 μL sample with 45 μL of 1× Tris-EDTA buffer (TE). For the PicoGreen assay, 10 μL of the sample was applied in four replicates (two for the naive condition and two for the Triton X-100 condition). Two replicates of each prepared standard DNA sample were loaded into a 96-well microplate. Four replicates of each test sample (10 μL) were added with 40 μL of 1× TE into the 96-well microplate. In addition, 50 μL of 1× TE was added to

half of the replicates, and 50 μL of 4% Triton X-100 was added to the remaining replicates. The plate was shaken for 5 min at RT, avoiding light exposure. Fluorescence was measured using a microplate reader with an excitation wavelength of 480 nm and an emission wavelength of 520 nm. The concentration of nucleic acid outside the LNP was calculated using a standard curve. The concentration of nucleic acid inside the LNP was determined by subtracting the outside concentration from the total concentration. Encapsulation efficiency was then calculated as the ratio of the concentration of nucleic acid inside the LNP to the total nucleic acid concentration.

Immunohistochemistry

Mouse lung tissues were perfused with cold PBS and excised. The lung tissues were fixed in 4% PFA (catalog no. 163-20145, Wako) solution, embedded in paraffin, and cut into serial sections (4 μm thick). Paraffin sections (mouse lung and human lung) were stained with MT and H&E using standard protocols. MT staining was performed to detect collagen in connective tissues.

To assess TGF-β expression, immunohistochemistry (IHC) was performed on lung tissue sections using an IHC kit (catalog no. 879673, Invitrogen) according to the manufacturer's instructions. Images were obtained using a Leica light microscope.

To evaluate the therapeutic effect of the vector on PF, a pathologist performed histological analyses, including Ashcroft scoring, counting the number of inflammatory cells per unit area, measuring the percentage of the alveolar region occupied by collagen fibers, and evaluating TGF-β expression using IHC.

Multiplex analysis

BALF and cell supernatant were filtered through a 0.45-μm syringe filter (catalog no. SLHV R33 Rs, Millipore) and analyzed for inflammatory cytokines (TNF-α and IL-1β) using the Bio-Plex 200 system (Bio-Rad).

IF analysis

Cell preparation and staining

The cells (A549, HDF, and THP1) were plated on confocal dishes (catalog no. 801002, NEST), washed with PBS, and fixed with 4% PFA (catalog no. 163-20145, Wako) for 15 min. After washing with PBS, a blocking solution (5% normal horse serum, 0.01% TX-100 in PBS) was applied at RT for 30 min. The cells were incubated overnight at 4°C with primary antibodies. After incubation, the cells were washed and incubated again with secondary Alexa Fluor-conjugated antibodies (Invitrogen) and 4′,6-diamidino-2-phenylindole (DAPI) for 1.5 h at RT. The cells were then washed with a washing solution (0.2% NP-40 in PBS), followed by PBS.

Mouse lung single cells and BALF cells

Dissociated mouse lung single cells and BALF cells were attached to slides using cytospin (2×10^5/200 μL, 1,000 rpm, 5 min) after fixation with 4% PFA for 15 min. After washing with PBS, a blocking solution (5% normal horse serum, 0.01% Triton X-100 in PBS) was applied at RT for 30 min. The cells were incubated overnight at 4°C with primary antibodies. After incubation, the cells were washed and incubated again with secondary Alexa Fluor-conjugated antibodies (Invitrogen) and DAPI for 1.5 h at RT. The cells were then washed with a washing solution (0.2% NP-40 in PBS), followed by PBS.

Human lung slides

Human lung slides (normal and fibrosis) were provided by the Department of Pathology, Seoul National University Hospital, and purchased from Superbiochips Laboratories, Cancer Research Institute, Seoul National University. This study was approved by the IRB of Seoul National University Hospital (IRB no. 2101-023-1185).

Paraffin-embedded tissue sections

The paraffin-embedded tissue sections (human and mouse lung) were deparaffinized with xylene and rehydrated with graded alcohol. Sections were exposed to a heat-mediated antigen retrieval buffer (catalog no. ab93684, Abcam, or catalog no. S2368, Dako) and then blocked with 5% normal horse serum in PBS containing 0.01% Triton X-100 to block non-specific binding sites. The sections were incubated overnight at 4°C with primary antibodies. The slides were then incubated with secondary Alexa Fluor-conjugated antibodies (Invitrogen) and DAPI for 1.5 h at RT after washing. The slides were washed with a washing solution (0.2% NP-40 in PBS) and mounted in a fluorescence mounting medium (catalog no. S3023, Dako). Images were obtained using a Leica confocal microscope (TCS SP8).

OCT-embedded tissue sections

Human and mouse PCLSs were fixed with 4% PFA at RT for 15 min. The slices were immersed in 15% sucrose in PBS for 2 h and then transferred to 30% sucrose in PBS for overnight incubation in a cold room. Next, the slices were embedded in an OCT compound and sectioned into 8-μm-thick slices using a cryotome.

The slices were air-dried for 5 min and then blocked using a blocking solution (5% normal horse serum, 0.01% TX-100 in PBS) for 30 min at RT. The cells were incubated overnight at 4°C with primary antibodies. After incubation, the slices were washed and incubated again with secondary Alexa Fluor-conjugated antibodies (Invitrogen) and DAPI for 1.5 h at RT. The slides were washed with a washing solution (0.2% NP-40 in PBS) and mounted in a fluorescence mounting medium (catalog no. S3023, Dako). Images were obtained using a Leica confocal microscope (TCS SP8).

Quantitative reverse-transcription PCR analysis

Total RNA was first isolated from the cultured cells with TRIzol (catalog no. 15596026, Thermo Fisher Scientific) and then extracted according to the manufacturer's instructions. cDNA was synthesized from 1 μg RNA using Reverse Transcription Master Premix (catalog no. FSQ-201, Toyobo). The samples with FastStart Universal SYBR Green Master (Rox) (catalog no. 04 913 914 001, Roche) were run in a QuantStudio 5 sequence detection system (Applied Biosystems). GAPDH, peptidylprolyl isomerase A (PPIA), and β2 microglobulin

(B2M) were used as internal controls to calculate relative changes in gene expression. Primers were designed using the Primer BLAST tool (NCBI) and synthesized by Macrogen (Seoul, Korea).

The following primers were used:

GAPDH: forward: 5′-AAGGTCGGAGTCAACGGATTT-3′, reverse: 5′-GTTCTCAGCCTTGACGGTGC-3′

PPIA: forward: 5′-CATAATGGCACTGGTGGCAAG-3′, reverse: 5′-GCCATCCAACCACTCAGTCTT-3′

SNAI1: forward: 5′- TAGCGAGTGGTTCTTCTGCG -3′, reverse: 5′- TGCTGGAAGGTAAACTCTGGA-3′

SNAI2: forward: 5′- TTCGGACCCACACATTACTT -3′, reverse: 5′- CTTCTCCCCCCGTGTGAGTTCT -3′

CDH2: forward: 5′- CTTGCCAGAAAACTCCAGGG-3′, reverse: 5′- TGTGCCCTCAAATGAAACCG -3′

CDH1: forward: 5′- AGGCCAAGCAGCAGTACATT -3′, reverse: 5′- AAAGTCCTCGGACACTTCCA -3′

VIM: forward: 5′- AAATGGCTCGTCACCTTCGT-3′, reverse: 5′- AGAAATCCTGCTCTCCTCGC-3′

ACTA2: forward: 5′-GGCAAGTGATCACCATCGGA-3′, reverse: 5′-TCTCCTTCTGCATTCGGTCG-3′

TRIM33: forward: 5′-CTCCGGGATCATCAGGTTTA-3′, reverse: 5′-TCAACATGCAAGCACTCCTC-3′

COL1A1: forward: 5′-CTGCCGTGACCTCAAGATGT-3′, reverse: 5′-CCGAACCAGACATGCCTCTT-3′

TNF: forward: 5′- CTTCTGCCTGCTGCACTTTG -3′, reverse: 5′- GGGTTTGCTACA ACATGGGC-3′

IL1B: forward: 5′- CAGAAGTACCTGAGCTCGCC -3′, reverse: 5′- GTCCTGGAAGGA GCACTTCA-3′

Gapdh: forward: 5′- GAGTGTTTCCTCGTCCCGTAGA-3′, reverse: 5′- AATGAAGGGGTCGTTGATGG-3′

Ppia: forward: 5′-AGACAAAGTTCCAAAGACAGC -3', reverse: 5′-CGTAGATGGACCTGCCGC-3′

B2m: forward: 5′-GTATGCTATCCAGAAAACCCCTC-3′, reverse: 5′-GTTCTTCAGCATTTGGATTTCAAT-3′

Vim: forward: 5′- AGACCAGAGATGGACAGGTGA-3', reverse: 5′- TCTTGCGCTCCTGAAAAACTG-3′

Acta2: forward: 5′-ATCTTTCATTGGGATGGAGTCAG-3′, reverse: 5′-CTGTCAGCAATGCCTGGGTA-3′

Col1a1: forward: 5′-GATGGTGCCAAGGGTGATACT-3′, reverse: 5′-GGAGAACCATCAGCACCTTTG-3′

Flow cytometry analysis

Transfection efficacy of LipoDo in 293T

To confirm the transfection efficacy of LipoDo *in vitro*, 293T cells were plated in 6-well plates at a density of 3×10^5 cells per well. The following day, prepared lipofectants were used to transfect the cells with plasmid DNA at concentrations of 2, 4, and 8 μg. The next day, the cells were detached using trypsin and analyzed using a BD FACS Aria III (Becton Dickinson).

Transfection efficacy of LipoDo in the lung

To assess the transfection efficacy of LipoDo in the lung, the mouse lung was dissociated into single cells using a lung dissociation kit (catalog no. 130-095-927, Miltenyi Biotec). The mouse lung was dissociated using the enzyme included in the kit and the gentleMACS device under 37°C_m_LDK_1 conditions. The separated single cells were treated with red blood cell (RBC) lysis buffer to remove RBCs and then reconstituted in FACS buffer (2% FBS, 1% BSA in PBS). The separated single cells were incubated with the anti-GFP-488 (catalog no. A21311, Thermo Fisher Scientific) antibody. Flow cytometric analysis was performed using BD FACS Aria III (Becton Dickinson).

AM and IM analysis in whole lung

To analyze AMs and IMs in the lung, the mouse lung was dissociated into single cells using a lung dissociation kit (catalog no. 130-095-927, Miltenyi Biotec). The lung tissue was enzymatically digested with the kit-provided enzyme using a gentleMACS Octo Dissociator under 37°C_m_LDK_1 conditions. The dissociated cells were treated with RBC lysis buffer (Thermo Fisher Scientific) to eliminate RBCs and then reconstituted in FACS buffer (2% FBS, 1% BSA in PBS). The single cells were incubated with fluorophore-conjugated antibodies to identify macrophage subpopulations. Flow cytometric analysis was performed using BD FACS Symphony S6 (Becton Dickinson).

Cells were first gated for singlets based on FSC-H (Forward Scatter Height) vs. FSC-A (Forward Scatter Area) and SSC-H (Side Scatter Height) vs. SSC-A (Side Scatter Area). Immune cells were selected by gating $CD45^+$ populations, followed by exclusion of granulocytes ($Ly6G^-$). AMs were defined as $CD45^+$ $Ly6G^-$ $SiglecF^+$. Among $SiglecF^-$ cells, IMs were identified as $CD45^+$ $Ly6G^-$ $SiglecF^-$ $F4/80^+$. IMs were further classified into M1 macrophages ($CD45^+$ $Ly6G^-$ $SiglecF^-$ $F4/80^+$ $MHCII^+$) and M2 macrophages ($CD45^+$ $Ly6G^-$ $SiglecF^-$ $F4/80^+$ $MHCII^-$).

coIP analysis

To directly examine whether TIF1-γ interferes with the SMAD3-SMAD4 complex formation in response to TGF-β, coIP was performed in A549 cells overexpressing TIF1-γ. A549 cells were transduced with TIF1-γ lentivirus (VectorBuilder), and 1 h after treatment with 10 ng/mL rhTGF-β (catalog no. 7754-BH-005, R&D Systems), cells were harvested for analysis.

Cells were lysed using a manually prepared IP lysis buffer (20 mM Tris-HCl pH 7.5, 150 mM NaCl, 1% NP-40, 1 mM EDTA, and protease and phosphatase inhibitors), and 500 μL lysate containing 1.5 mg total protein was used for each immunoprecipitation. For

each sample, 2 μg anti-SMAD3 antibody was added to the lysate and incubated overnight at 4°C with rotation. The next day, 50 μL Protein A/G agarose beads (catalog no. ab193262, Abcam) was added to each tube and rotated for 3 h at 4°C.

Beads were washed three times with ice-cold IP washing buffer (20 mM Tris-HCl pH 7.5, 300 mM NaCl, 0.1% Tween 20), and samples were eluted by adding 2× sodium dodecyl sulfate (SDS) loading buffer followed by boiling. A portion of the lysate (5%) was reserved as input control. Both input and IP samples were analyzed by western blot.

Western blot analysis

Total protein was extracted from cells using radioimmunoprecipitation assay cell lysis buffer (catalog no. 89901, Thermo Fisher Scientific) supplemented with complete protease inhibitor (catalog no. P3100-001, GenDEPOT) and phosphatase inhibitor (catalog no. P3200-001, GenDEPOT) cocktails. The lysates were incubated on ice for 15 min and then centrifuged at 13,000 rpm and 4°C for 10 min. The protein concentration was determined using a bicinchoninic acid assay (catalog no. 23223, Thermo Fisher Scientific). Proteins were separated using 10% SDS-polyacrylamide gel electrophoresis and transferred onto a polyvinylidene fluoride membrane using an iBlot 2 gel transfer device (catalog no. IB24001, Thermo Fisher Scientific). The membrane was blocked with 5% normal horse serum in PBS and incubated overnight at 4°C with primary antibodies. The membrane was washed and incubated with horseradish peroxidase (HRP)-conjugated secondary antibodies. Secondary antibodies were washed out after incubation. The immunoreactive bands were detected using an enhanced chemiluminescence HRP chemiluminescent substrate. Proteins from the western blot were quantified using ImageJ.

Statistical analysis

The statistical analysis was performed using GraphPad Prism 8 software (GraphPad Software). Data are presented as the mean ± standard deviation (SD). Differences between groups were analyzed using unpaired two-tailed Student's t test (for comparisons between two groups) or one-way analysis of variance followed by Sidak's multiple comparisons test (for comparisons among three or more groups). $^{*}p < 0.05$, $^{**}p < 0.01$, $^{***}p < 0.001$, and $^{****}p < 0.0001$ were considered statistically significant.

DATA AVAILABILITY

The raw/processed data required to reproduce these findings are available upon request.

ACKNOWLEDGMENTS

This research was supported by a grant of the Korea Health Technology R&D Project through the Korea Health Industry Development Institute (KHIDI), funded by the Ministry of Health & Welfare, South Korea (grant no. HI14C1277). This study also received funding support from the Ministry of Education, Singapore (grant no. MOE-MOET32022-0002). The funder had no role in the study design, data collection and analysis, decision to publish, or preparation of the manuscript.

AUTHOR CONTRIBUTIONS

Study concept and design: E.J.L., D.M., and H.-S.K. Acquisition, analysis, or interpretation of data: all authors. Drafting of the manuscript: E.J.L., D.M., and H.-S.K. Preparation of materials: K.A., T.K., and N.J.C. Critical revision of the manuscript for important intellectual content: all authors. Pathology specimen and review: J.-Y.K., S.P., J.K., and S.-H.P. Funding acquisition: E.J.L. and H.-S.K.

DECLARATION OF INTERESTS

The authors declare no competing interests.

SUPPLEMENTAL INFORMATION

Supplemental information can be found online at https://doi.org/10.1016/j.ymthe.2025.08.035.

REFERENCES

1. Koudstaal, T., Funke-Chambour, M., Kreuter, M., Molyneaux, P.L., and Wijsenbeek, M.S. (2023). Pulmonary fibrosis: from pathogenesis to clinical decision-making. Trends Mol. Med. *29*, 1076–1087. https://doi.org/10.1016/j.molmed.2023.08.010.

2. Raghu, G., Remy-Jardin, M., Richeldi, L., Thomson, C.C., Inoue, Y., Johkoh, T., Kreuter, M., Lynch, D.A., Maher, T.M., Martinez, F.J., et al. (2022). Idiopathic Pulmonary Fibrosis (an Update) and Progressive Pulmonary Fibrosis in Adults: An Official ATS/ERS/JRS/ALAT Clinical Practice Guideline. Am. J. Respir. Crit. Care Med. *205*, e18–e47. https://doi.org/10.1164/rccm.202202-0399ST.

3. Richeldi, L., Collard, H.R., and Jones, M.G. (2017). Idiopathic pulmonary fibrosis. Lancet *389*, 1941–1952. https://doi.org/10.1016/S0140-6736(17)30866-8.

4. Martinez, F.J., Collard, H.R., Pardo, A., Raghu, G., Richeldi, L., Selman, M., Swigris, J.J., Taniguchi, H., and Wells, A.U. (2017). Idiopathic pulmonary fibrosis. Nat. Rev. Dis. Primers *3*, 17074. https://doi.org/10.1038/nrdp.2017.74.

5. Glass, D.S., Grossfeld, D., Renna, H.A., Agarwala, P., Spiegler, P., DeLeon, J., and Reiss, A.B. (2022). Idiopathic pulmonary fibrosis: Current and future treatment. Clin. Respir. J. *16*, 84–96. https://doi.org/10.1111/crj.13466.

6. Parimon, T., Yao, C., Stripp, B.R., Noble, P.W., and Chen, P. (2020). Alveolar Epithelial Type II Cells as Drivers of Lung Fibrosis in Idiopathic Pulmonary Fibrosis. Int. J. Mol. Sci. *21*, 2269. https://doi.org/10.3390/ijms21072269.

7. Fernandez, I.E., and Eickelberg, O. (2012). The impact of TGFbeta on lung fibrosis: from targeting to biomarkers. Proc. Am. Thorac. Soc. *9*, 111–116. https://doi.org/10.1513/pats.201203-023AW.

8. Denton, C.P., Goh, N.S., Humphries, S.M., Maher, T.M., Spiera, R., Devaraj, A., Ho, L., Stock, C., Erhardt, E., Alves, M., and Wells, A.U. (2023). Extent of fibrosis and lung function decline in patients with systemic sclerosis and interstitial lung disease: data from the SENSCIS trial. Rheumatology (Oxford) *62*, 1870–1876. https://doi.org/10.1093/rheumatology/keac535.

9. Allanore, Y., Vonk, M.C., Distler, O., Azuma, A., Mayes, M.D., Gahlemann, M., James, A., Kohlbrenner, V., Alves, M., Khanna, D., et al. (2022). Continued treatment with nintedanib in patients with systemic sclerosis-associated interstitial lung disease: data from SENSCIS-ON. Ann. Rheum. Dis. *81*, 1722–1729. https://doi.org/10.1136/ard-2022-222564.

10. Cerri, S., Monari, M., Guerrieri, A., Donatelli, P., Bassi, I., Garuti, M., Luppi, F., Betti, S., Bandelli, G., Carpano, M., et al. (2019). Real-life comparison of pirfenidone and nintedanib in patients with idiopathic pulmonary fibrosis: A 24-month assessment. Respir. Med. *159*, 105803. https://doi.org/10.1016/j.rmed.2019.105803.

11. Lee, E.J., Hwang, I., Lee, J.Y., Park, J.N., Kim, K.C., Kim, I., Moon, D., Park, H., Lee, S.Y., Kim, H.S., et al. (2020). Hepatic stellate cell-specific knockout of transcriptional intermediary factor 1gamma aggravates liver fibrosis. J. Exp. Med. *217*, e20190402. https://doi.org/10.1084/jem.20190402.

12. Moon, D., Park, H., Hwang, I., Cha, A., Yun, H., Lee, J., Park, S.H., Lee, E.J., and Kim, H.S. (2022). Smart gene therapeutics for selective targeting of myofibroblasts derived from hepatic stellate cells and limited expression under inflamed conditions. Clin. Transl. Med. *12*, e991. https://doi.org/10.1002/ctm2.991.

13. Xue, J., Chen, Y., Wu, Y., Wang, Z., Zhou, A., Zhang, S., Lin, K., Aldape, K., Majumder, S., Lu, Z., and Huang, S. (2015). Tumour suppressor TRIM33 targets nuclear beta-catenin degradation. Nat. Commun. *6*, 6156. https://doi.org/10.1038/ncomms7156.

14. Barkauskas, C.E., Cronce, M.J., Rackley, C.R., Bowie, E.J., Keene, D.R., Stripp, B.R., Randell, S.H., Noble, P.W., and Hogan, B.L.M. (2013). Type 2 alveolar cells are stem cells in adult lung. J. Clin. Invest. *123*, 3025–3036. https://doi.org/10.1172/JCI68782.

15. Willis, B.C., and Borok, Z. (2007). TGFbeta-induced EMT: mechanisms and implications for fibrotic lung disease. Am. J. Physiol. Lung Cell. Mol. Physiol. *293*, L525–L534. https://doi.org/10.1152/ajplung.00163.2007.

16. Foster, K.A., Oster, C.G., Mayer, M.M., Avery, M.L., and Audus, K.L. (1998). Characterization of the A549 cell line as a type II pulmonary epithelial cell model for drug metabolism. Exp. Cell Res. *243*, 359–366. https://doi.org/10.1006/excr.1998.4172.

17. Mendonca, M.C.P., Kont, A., Kowalski, P.S., and O'Driscoll, C.M. (2023). Design of lipid-based nanoparticles for delivery of therapeutic nucleic acids. Drug Discov. Today *28*, 103505. https://doi.org/10.1016/j.drudis.2023.103505.

18. Hattori, Y., Nakamura, M., Takeuchi, N., Tamaki, K., Shimizu, S., Yoshiike, Y., Taguchi, M., Ohno, H., Ozaki, K.I., and Onishi, H. (2019). Effect of cationic lipid in cationic liposomes on siRNA delivery into the lung by intravenous injection of cationic lipoplex. J. Drug Target. *27*, 217–227. https://doi.org/10.1080/1061186X.2018.1502775.

19. Chang, H.I., and Yeh, M.K. (2012). Clinical development of liposome-based drugs: formulation, characterization, and therapeutic efficacy. Int. J. Nanomedicine *7*, 49–60. https://doi.org/10.2147/IJN.S26766.

20. Farkas, L., Farkas, D., Ask, K., Möller, A., Gauldie, J., Margetts, P., Inman, M., and Kolb, M. (2009). VEGF ameliorates pulmonary hypertension through inhibition of endothelial apoptosis in experimental lung fibrosis in rats. J. Clin. Invest. *119*, 1298–1311. https://doi.org/10.1172/JCI36136.

21. Viana, F., O'Kane, C.M., and Schroeder, G.N. (2022). Precision-cut lung slices: A powerful ex vivo model to investigate respiratory infectious diseases. Mol. Microbiol. *117*, 578–588. https://doi.org/10.1111/mmi.14817.

22. Liu, G., Betts, C., Cunoosamy, D.M., Åberg, P.M., Hornberg, J.J., Sivars, K.B., and Cohen, T.S. (2019). Use of precision cut lung slices as a translational model for the study of lung biology. Respir. Res. *20*, 162. https://doi.org/10.1186/s12931-019-1131-x.

23. Kolanko, E., Cargnoni, A., Papait, A., Silini, A.R., Czekaj, P., and Parolini, O. (2024). The evolution of in vitro models of lung fibrosis: promising prospects for drug discovery. Eur. Respir. Rev. *33*, 230127. https://doi.org/10.1183/16000617.0127-2023.

24. Wijsenbeek, M., Suzuki, A., and Maher, T.M. (2022). Interstitial lung diseases. Lancet *400*, 769–786. https://doi.org/10.1016/S0140-6736(22)01052-2.

25. Henderson, N.C., Rieder, F., and Wynn, T.A. (2020). Fibrosis: from mechanisms to medicines. Nature *587*, 555–566. https://doi.org/10.1038/s41586-020-2938-9.

26. Bender, E. (2018). Regulating the gene-therapy revolution. Nature *564*, S20–S22. https://doi.org/10.1038/d41586-018-07641-1.

27. Collins, F.S., and Gottlieb, S. (2018). The Next Phase of Human Gene-Therapy Oversight. N. Engl. J. Med. *379*, 1393–1395. https://doi.org/10.1056/NEJMp1810628.